AVANCES
EN CIENCIAS E INGENIERÍAS
ARTÍCULO/ARTICLE SECCIÓN/SECTION C

Spatial Variability of Water Retention Curve Fractal Dimension

Samuele De Bartolo[1*], Carmine Fallico[1], María Fernanda Rivera-Velasquez[2], Massimo Veltri[1]

[1] *Università della Calabria, Dipartimento di Ingegneria Civile, Ponte P. Bucci Cubo 41 B, 87036, Rende, Italia.*
[2] *Universidad Nacional de Chimborazo, Facultad de Ingeniería, Avenida Antonio José de Sucre, EC060104 Riobamba, Ecuador.*
** Autor principal/Corresponding author, e-mail: samuele.debartolo@unical.it*

Editado por/Edited by: Cesar Zambrano, Ph.D.
Recibido/Received: 2015/10/16. Aceptado/Accepted: 2015/11/20.
Publicado en línea/Published on Web: 2015/12/30. Impreso/Printed: 2015/12/30.

Variabilidad Espacial de Dimensiones Fractales en Curvas de Retención de Agua

Abstract

The study of spatial variability of specific quantities characterizing the unsaturated soil is very important for the evaluation of polluting phenomena. Geostatistics is a useful tool for estimating the spatial variability of the considered parameters. The aim of this study is to improve the understanding of the spatial variability of the fractal dimension of water retention curves, showing the behaviour of this parameter in the site examined and particularly at the points where measures were not performed. The assessment of the fractal dimension was calculated by the analysis of scaling obtained from some fractal models and a comparison among the correspondent results was performed.

Keywords. Water Retention Curves, Geostatistics, Fractal Dimension, Scaling Analysis.

Resumen

El estudio de la variabilidad espacial de específicas magnitudes que caracterizan el suelo no saturado es muy importante para la evaluación de los fenómenos de contaminaciòn. La Geoestadística es una herramienta útil para la estimación de la variabilidad espacial de los parámetros considerados. El objetivo de este estudio es mejorara la comprensión de la variabilidad espacial de la dimensión fractal en las curvas de retención de agua, mostrando de esta manera el comportamiento de este parámetro en los puntos muestreados y de manera particular en los puntos donde no existen muestras. La evaluación de la dimensión fractal se calculó por el análisis de escalamiento obtenido a partir de algunos modelos fractales y la posterior comparación entre los resultados correspondientes.

Palabras Clave. Curvas de retención del agua, Geoestadística, Dimensión Fractal, Análisis de escalamiento.

Introduction

By using fractal geometry to characterise pore space, groundwater behaviour can be effectively related to the water and structural properties in the soil. The available field and laboratory methods that are able to define correctly the properties of unsaturated soil are very expensive and time-consuming. In the literature there are many models that can interpret various phenomena by fractal geometry characterising the porous media, such as water retention curves (WRC) and hydraulic conductivity [1]. These models were the outcome of theoretical and experimental studies designed to describe soil fractal structure in terms of soil particle size distribution [2], solid aggregate typology distribution [3, 4], pore-solid interface area [5], pore-phase fractal mass [6, 7] and solid-phase fractal mass [8–10]. Essentially, the basic fractal scheme used in these models to describe soil fractal scaling behaviour in terms of either the solid or the pore phase is the Menger sponge [5, 11, 12]. These models are characterized by a single geometric parameter that represents a scale invariant, namely, the fractal dimension (D_f) [11]. Different studies [2, 5, 8, 9, 11, 12] show that in the porous media the scaling law represents a connection among water contained, matrix potential and the porous medium. Therefore, the valuation of the fractal dimension is very important on the field scale, because this value is correlated to the scale process of WRC at the single point of measure. In fact, it could be of great interest to have not only information on WRC in each location where the sampling was carried out, but, obviously, also at other points where this measure was not performed. For this purpose, the geostatistic [13, 14] offers a group of methods to describe quantitatively the spatial continuity that is an essential feature of many natural phenomena [15, 16]. Therefore

ISSN 1390-5384

this approach allows the fractal dimension to be considered as a random function and to be represented on the field scale of the measures. The fractal dimension distribution is performed beginning from the knowledge of the WRC in a limited series of points on the specific area investigated. That allows useful information to be obtained about the fractal dimension values also at points where the measurements are lacking. The comparison among the results obtained in this way by the fractal models permits interesting considerations on the availability of these for the retention curve description.

Materials and Methods

Description of investigation area

The site where the measurements took place is an experimental field of the Turbolo basin in Calabria, Italy (Fig. 1), which furnishes the data set for the spatial characterisation of the fractal dimension through geostatistical analysis. This site covers an area of 2800 m^2 (70 x 40 metres) and a specific instrumentation was used for continuous monitoring, at various locations and at different depths. To characterize the unsaturated soil, an experimental field was selected with a rectangular surface of 800 m^2 (40 x 20 metres), sloping lengthwise at a gradient of about 6%. Metallic cylinders 0.05 metres in diameter and 0.051 metres high, with a sharp bottom rim for better penetration, were pressed vertically into the undisturbed soil to take a total of 30 cores. Fig. 1 shows the locations where the undisturbed soil cores were extracted. These samples were analysed in the laboratory, where the particle size distribution, the bulk density, the saturated hydraulic conductivity and the water content at different pressure heads were determined to plot the WRC, by using the conventional Richards apparatus.

Fractal models for WRC definition

The use of WRC fractal models and the spatial interpolation methods allows indications to be obtained about

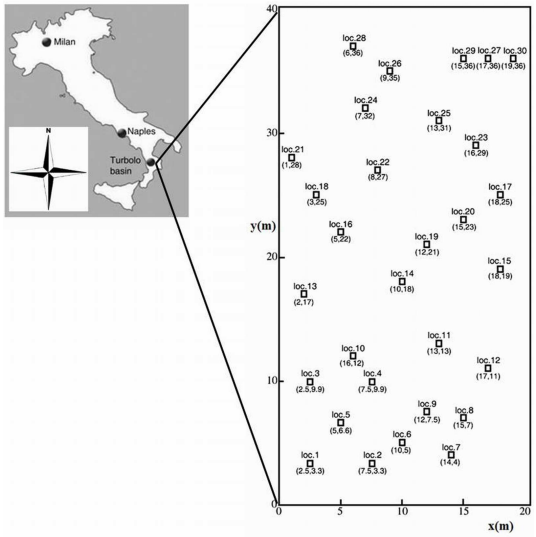

Figure 1: Turbolo River and experimental field.

the soil spatial variability i. e. of the characteristic soil parameters, specifically of the D_f. The literature shows that fractal geometry has been successfully used to interpret water retention and the variability of hydraulic conductivity in soils with different textural structures [4, 17, 18]. Among the existing fractal models and according to Perfect et al. [19] the WRC are commonly grouped in three classes namely the Tyler and Wheatcraft [20] (TW), the Rieu and Sposito [8, 9] (RS) and the Perrier et al. [22] pore solid fractal (PSF) models.

The model of Tyler and Wheatcraft [20] is based on a two-dimensional Sierpiński carpet stretched to form a capillary bundle, and is easily extensible to three dimensions. This model is applied within the limit of infinite iterations when the porosity is unity. The analytic expression of TW model is the following:

$$\theta(h) = \theta_S \left(\frac{h}{h_{\min}} \right)^{D_f - 3} \tag{1}$$

where θ_S is the saturated water content, h is the generic water potential, h_{min} is the water potential commonly named air-entry value [21] and D_f is the fractal dimension.

The Rieu and Sposito [8, 9] model treats the WRC as a partially fragmented porous medium with porosity less than or equal to 1. This model can be represented by the following relation:

$$\theta(h) = \theta_S - 1 + \left(\frac{h}{h_{\min}} \right)^{D_f - 3} \tag{2}$$

where the parameters assume the same mean as shown above.

The model of Perrier et al. [22], known as the pore-solid fractal (PSF) model, represents a generalization of the solid and pore mass fractal models. Similarly to the TW and RS models, the PSF model characterises both the solid and pore phases of the porous media. It also exhibits self-similarity to a degree, in the sense that where local structure occurs, it is seen to be similar to the whole structure [12].

According to Bird et al. [12], the PSF model can be represented by the following relation:

$$\theta(h) = (\theta_S - A) - A \left(\frac{h}{h_{\min}} \right)^{D_f - 3} \tag{3}$$

In equation (3) the parameter A is defined as [23]:

$$A = \frac{p}{p + s} \tag{4}$$

where p and s are the pore and solid phase fractions at each scale. This parameter is variable between the saturated water content (θ_S) and 1 (i.e. $\theta_S \leq A \leq 1$).

Evaluating the (1), (2) and (3) expressions, the fractal dimension can be estimated by analysing the log-log plots of θ^* versus (h_{min}/h), in which $log\theta^*$ is defined as follows:

$$\log\theta^* = \log\frac{\theta}{\theta_s}; \log\theta^* = \log\left(\theta + 1 - \theta_s\right); \quad \log\theta^* = \log\frac{\theta+A-\theta_s}{A} \tag{5}$$

respectively for the TW, RS and PSF models. More precisely, D_f is calculated in the scaling range that is delimited by lower $log\left(h/h_{min}\right)_{inf}$ and upper $log\left(h/h_{min}\right)_{sup}$ values, where the determination coefficient R^2 of the regression curve is maximum. Commonly for each WRC, it is possible to identify two scaling ranges: one lower for very low water content and the other upper for larger water contents [5, 11, 24, 25].

Assessment of the fractal dimension

The individualization of fractal dimension distribution can be carried out considering the scaling procedure defined in Fallico et al. [25], analysing the log-log plots of θ^* versus (h_{min}/h), in which $log\theta^*$ is defined for each fractal model by relations (5).

Specifically, according to experimental studies by Toledo et al. [5], Millàn and Gonzàles-Posada [24] and Fallico et al. [25], it is possible to define two scaling ranges of the WRC, one for the larger and the other for the smaller water contents. In this context the fractal dimension can be defined, for each of the two scaling ranges, as the slope of the straight regression line interpolating the experimental WRC points with the highest coefficient of determination R^2 [26]. This procedure allows the scaling range to be determined in which the fractal dimension is an invariant of scale. The WRC models considered in the present study are the three represented by the relationships (1), (2) and (3) above shown. Since the methodology of the fractal analysis and also the results are those reported in Fallico et al. [25], where all the setting values are defined, the reader should refer to this study for all details. Altogether, ten data sets of the fractal dimensions were considered, specifically, five samples are related to the lower range (I) and the others represent the upper range (II). These values include also the three relative to the PSF model, with A=0.30, A=0.45 and A=0.60, that are representative of the examined unsaturated soil [25]. This was carried out for each location. By means of a geostatistics analysis performed for each model data set to individualise the spatial distribution of the fractal dimension, in the present study we checked the reliability of the models and defined that showing the best fitting of the measured values. This latter approach can be considered an extention of the investigation carried out previously by Fallico et al. [25].

Geostatical analysis

The theoretical basis of the geostatistics was described by several authors [16, 27]. This procedure represents a class of statistical techniques developed to analyse and predict values of a variable distributed in space or time. Generally, geostatistics is accepted as a science to study the random and structural character or spatial autocorrelation [28] of natural phenomena with the support of Regionalized Variables Theory and variograms [13, 16].

The exploratory data analysis (EDA) is the preliminary phase of geostatistical analysis. This procedure identifies the principal parameters of descriptive statistic performing a graphical description of the data set (Boxplot, Q-Q plot etc.). Then the EDA represents a good method to locate anomalous values (outliers) [29] and to verify the existence of outliers by statistics tests [30]. In the geostatistics a normal and/or lognormal distribution of the variable understudy is desirable when the hypothesis of stationarity occurs [31] and different hypothesis tests can be considered [32, 33] to effect the verification of this hypothesis. In geostatistics, the modeling of spatial data is accomplished through the calculation of the experimental variogram, showing the increase in variability between sample locations and a generic point. The variogram describes the spatial relationship between the sample values as a function that relates the variance (γ) to the distance of sample separations (d) usually called lag. The variogram equation is given as [13]:

$$\gamma\left(d\right) = \frac{1}{2N\left(d\right)}\sum_{i=1}^{N(d)}\left[z\left(u_i\right) - z\left(u_i + d\right)\right]^2 \tag{6}$$

where $N(d)$ is the number of sample pairs [13, 34], $\gamma(d)$ is the semivariance, $z(u_i)$ and $z(u_i + d)$ are the observation values of the studied variable measured at point u_i and at a point separated by d vector, respectively. To verify the presence of eventual anisotropy in the data, often the variogram surface [16] and/or the directional variograms [14, 15] are usually displayed. The anisotropy of the variogram surface (these values tend to be more similar in one or more preferred directions than in others) reveals a covariance structure that is usually related to the orientation of natural phenomena acting in the studied area; the directional variograms reveal the changes in the variogram parameters as the direction changes when the phenomenon is anisotropic. The experimental variogram is commonly fitted by using a mathematical equation [15, 16] whose main parameters are sill (C) or partial sill (C_1), range (A) and nugget (C_0). The variogram model is a curved line through the experimental variogram points. Afterwards, the interpolation phase is commonly performed to obtain the spatial distribution of the investigated parameter according to the purpose of the geostatistical methodology. In the field of Earth Sciences this phase is named kriging, which is one of the most commonly used estimation techniques that uses variogram model parameters. It is a

Fractal Model	Min.	Max.	Mean	Median	Stand. Error	Stand. Dev.	Var.	Kurt.	Skew.
TW(I)	2.8943	2.9779	2.9509	2.9530	$3.30{\cdot}10^{-3}$	$1.80{\cdot}10^{-2}$	$3.30{\cdot}10^{-4}$	3.5408	-1.5992
RS(I)	2.9630	2.9931	2.9836	2.9842	$1.18{\cdot}10^{-3}$	$6.50{\cdot}10^{-3}$	$4.22{\cdot}10^{-5}$	3.2441	-1.5044
PSF0.30(I)	2.8468	2.9731	2.9327	2.9323	$4.81{\cdot}10^{-3}$	$2.59{\cdot}10^{-2}$	$6.72{\cdot}10^{-4}$	2.9248	-1.1723
PSF0.45(I)	2.8964	2.9834	2.9583	2.9603	$3.32{\cdot}10^{-3}$	$1.82{\cdot}10^{-2}$	$3.31{\cdot}10^{-4}$	4.3097	-1.7475
PSF0.60(I)	2.9305	2.9880	2.9706	2.9719	$2.23{\cdot}10^{-3}$	$1.22{\cdot}10^{-2}$	$1.49{\cdot}10^{-4}$	3.7734	-1.6387
TW(II)	2.7423	2.8362	2.7782	2.7715	$5.06{\cdot}10^{-3}$	$2.63{\cdot}10^{-2}$	$6.93{\cdot}10^{-4}$	-0.1022	0.8807
RS(II)	2.9388	2.9616	2.9476	2.9468	$9.22{\cdot}10^{-4}$	$4.79{\cdot}10^{-3}$	$2.29{\cdot}10^{-5}$	1.4767	0.8048
PSF0.30(II)	2.1094	2.6960	2.5322	2.5688	$2.64{\cdot}10^{-2}$	1.37·10-1	$1.89{\cdot}10^{-2}$	1.9191	-1.2707
PSF0.45(II)	2.8063	2.8757	2.8342	2.8294	$3.30{\cdot}10^{-3}$	$1.71{\cdot}10^{-2}$	$2.94{\cdot}10^{-4}$	-0.1562	0.4601
PSF0.60(II)	2.8806	2.9229	2.8961	2.8952	$1.83{\cdot}10^{-3}$	$9.53{\cdot}10^{-3}$	$9.08{\cdot}10^{-5}$	1.001	0.6895

Table 1: Parameters of EDA (minimum, maximum, mean, median, standard error, standard deviation, variance, kurtosis, skewness) of sets derived from the D_f values calculated for the first (I) and second (II) range and for each considered fractal model.

method of interpolation which predicts unknown values from data observed at known locations and it minimizes the variance of the chosen linear combination of the data subject to the constraint that the estimator must be unbiased. In the present paper, the ordinary kriging [15, 16] is chosen to interpolate the punctual data of examinated variable. Assuming the intrinsic hypothesis, the linear system of ordinary kriging equations can be expressed as:

$$\begin{cases} \sum_{i=1}^{N} \lambda_i \gamma(u_i, u_j) + \mu = \gamma(u_i, u) \\ \sum_{i=1}^{n} \lambda_i = 1 \end{cases} \quad (7)$$

where λ_i is an unknown weight for the measured value at the *i* location, μ is Lagrange multiplier, $\gamma(u_i, u_j)$ is the value of variogram corresponding to a vector with origin in u_i and extremity u_j and $\gamma(u_i, u)$ represent the variogram between u_i and *u* (unsampled location). Moreover, to estimate the values at new locations, a statistical spatial prediction technique, producing a measure of the uncertainty associated with a given model, was utilized. In geostatistics, this is often referred to as the prediction variance, i.e. the estimated variance of the prediction error. The ordinary kriging variance is defined as [14]:

$$\sigma^2(u) = \sum_{i=1}^{n} \lambda_i \gamma(u_i, u) - \mu \quad (8)$$

This parameter depends on the data configuration but does not depend on the data values. To check the optimal adaptation of the variogram model (or theoretical) with the experimental variogram, a cross-validation was applied [35]. This procedure consists in the application of the spatial model selected to predict a value in each sampling point. The cross-validation compares the predicted and observed data; the difference between these values is called error of estimate. Two diagnostics statistics are performed to verify the reliability of the model. The mean deviation or mean error (*ME*) is given by the following expression:

$$ME = \frac{1}{N} \sum_{i=1}^{N} [z^*(u_i) - z(u_i)] \quad (9)$$

where $z^*(u_i)$ is the measured value at the *i* location and $z(u_i)$ the estimated value. The variance of standardised error (*VSE*) can be expressed as:

$$VSE = \frac{1}{N} \sum_{i=1}^{N} \frac{[z^*(u_i) - z(u_i)]^2}{\sigma^2(u_i)} \quad (10)$$

in which $\sigma^2(u_i)$ is the kriging variance. The *VSE* parameter corresponds to the relationship between the experimental and theoretical variance. If the variogram model is careful then the mean error should be ideally 0 because the kriging is unbiased, while the *VSE* value should be 1.

Results y Discussion

In Table 1 the parameters of EDA, comprising the D_f values calculated for the first (I) and second (II) range of scaling, are summarised for all the considered fractal models.

These results show that the RS model, for high (I) and low (II) water contents, has a medium value of fractal dimension equal to 2.9836 and 2.9476, respectively. Then for this fractal model the variable has the highest values. The averages of the data sets for high water contents are between 2.9327 and 2.9836, while for low water contents the average values are included in a larger range, that is, between 2.5322 and 2.9476. This situation leads to a first consideration of a consistent heterogeneity of fractal dimension values for the second range of scaling, even if the number of the experimental points for this range is very limited. Both for high and low water contents, the RS model shows the smallest values of variance that are $4.22{\cdot}10^{-5}$ and $2.29{\cdot}10^{-5}$, respectively, whereas the PSF model with *A*=0.30 has the largest values, $6.72{\cdot}10^{-4}$ and $1.89{\cdot}10^{-2}$.

Test	**TW (I)**		**RS (I)**		**PSF$_{0.30}$ (I)**		**PSF$_{0.45}$ (I)**		**PSF$_{0.60}$ (I)**	
	Norm.	Lognorm.	Norm.	Lognorm.	Norm.	Lognorm.	Norm.	Lognorm.	Norm.	Lognorm.
K-S	0.1596	0.1598	0.1403	0.1382	0.1194	0.1227	0.1572	0.1561	0.1483	0.1467
A-D	1.1204	1.1230	0.9560	0.9416	0.4776	0.4788	1.1417	1.1424	1.0607	1.0534
χ^2	1.5528	1.5531	1.6453	1.6474	0.16834	0.1800	0.8223	0.8198	0.8221	0.8224
Test	**TW (II)**		**RS (II)**		**PSF$_{0.30}$ (II)**		**PSF$_{0.45}$ (II)**		**PSF$_{0.60}$ (II)**	
	Norm.	Lognorm.	Norm.	Lognorm.	Norm.	Lognorm.	Norm.	Lognorm.	Norm.	Lognorm.
K-S	0.1596	0.1598	0.1403	0.1382	0.1194	0.1227	0.1572	0.1561	0.1483	0.1467
A-D	1.1204	1.1230	0.9560	0.9416	0.4776	0.4788	1.1417	1.1424	1.0607	1.0534
χ^2	1.5528	1.5531	1.6453	1.6474	0.1683	0.1800	0.8223	0.8198	0.8221	0.8224

Table 2: Numerical results of the K-S, A-D and χ^2 tests; (I) and (II) are the two scaling ranges of the high and low water contents, respectively.

The kurtosis coefficient is always positive for all the fractal models, therefore the data sets have a leptokurtic distribution. Only the TW and PSF with A=0.45 for low water contents differ because the curtosis coefficient is negative. For all the fractal models with high water contents and for the PSF model with A=0.30 and for low water contents, the skewness negative indicates that the mean is to the left of the median of the distributions. For the others fractal models this parameter is positive. To verify the assumption around the normal and/or lognormal distribution of the data sets, the Kolmogorov-Smirnov (K-S), Anderson-Darling (A-D) and Chi-Square (χ^2) hypothesis tests were used. Table 2 gives the results of these tests, for which the significance level α is 0.05. It can be verified that the statistical value always results smaller than the critical values that are 0.242, 2.502 and 7.815 for K-S, A-D and χ^2 tests, respectively. Then, all the data sets of D_f associated with each fractal model can be well interpreted with normal and log-normal distributions.

To check the presence of anomalous values in the data sets, the Dixon test was used. The statistic experimental parameter (Q_{exp}) is compared to a critical value (Q_{crit}) that is possible to find in specific tables [30] and for different values of the significance level (α). Table 3 gives the outliers values with respective locations and the results of the Dixon test for each fractal model and for high and low water contents.

Fractal Model	**Location**	**Outlier**	**Q_{exp}**	**Q_{crit} (α=0.1)**
TW(I)	2 26	2.89426 2.90098	0.4438	0.285
RS(I)	2 26	2.96688 2.96295	0.4310	0.285
PSF$_{0.30}$(I)	2	2.84677	0.3887	0.218
PSF$_{0.45}$(I)	2 26	2.9140 2.89643	0.4937	0.285
PSF$_{0.60}$(I)	2 26	2.94012 2.93053	0.4634	0.285
RS(II)	2	2.9616	0.340	0.224
PSF$_{0.30}$(II)	26	2.10942	0.3746	0.224
PSF$_{0.45}$(II)	2	2.8757	0.2282	0.224
PSF$_{0.60}$(II)	2	2.92292	0.3039	0.224

Table 3: Anomalous values (outliers) for each fractal model and results of the Dixon test.

Assuming a significance level α of 0.1, for all the data sets and for all the hypothesized outliers, the Q_{crit} parameter is smaller than the Q_{exp} value. Then, unlike the PSF model with A=0.30, each fractal model for the first range of scaling has anomalous values at the locations 2 and 26. These outliers are 2.89426 and 2.90098 for the TW model, 2.96688 and 2.96295 for the RS model, 2.84677 for the PSF model with A=0.30 at the location 2, 2.9140 and 2.89643 for the PSF model with A=0.45, 2.94012 and 2.93053 for the for the PSF model with A=0.60. For the second range of scaling, in the TW model there are no outliers. The RS, the PSF with A=0.45 and the PSF with A=0.60 models show outliers at location 2 that are 2.9616, 2.8757 and 2.92292, respectively. The PSF model with A=0.30 has an anomalous value of fractal dimension of 2.10942 at location 26. After a preliminary statistical study of the data sets, the results of the structural analysis are shown, which is based on the study of possible anisotropies, the construction of the experimental variogram and the relative model. The study of the directional variograms and of the variogram maps allows the D_f distribution to be considered as an isotropic phenomenon, for each fractal model and for the first and second range of scaling. For example, Fig. 2 displays the variogram map and the directional variograms for the RS fractal model and the first range of scaling. Analyzing the variogram map, it can be seen that the fractal dimension variable is a phenomenon distributed uniformly in any direction.

This circumstance was verified for each fractal model. The directional variograms was identified in East, North-East, North and North-West directions by an angular tolerance of 22.5°. Examining these variograms, it can be affirmed that they have a similar behaviour in each direction and do not reveal the changes of variogram parameters, which are: sill, range and nugget. In accordance with these results, the fractal dimension is an isotropic event and omnidirectional variograms were used to effect the geostatistical analysis. Table 4 shows the quantities that define the structural analysis for high and low water contents and for each fractal model, which are: lag, lag number, the variogram model and the respective parameters.

The lag is 3 metres for fractal models with high water contents, whereas for low water contents it assumes a value equal to 2.9 metres and 2.8 metres for TW and the

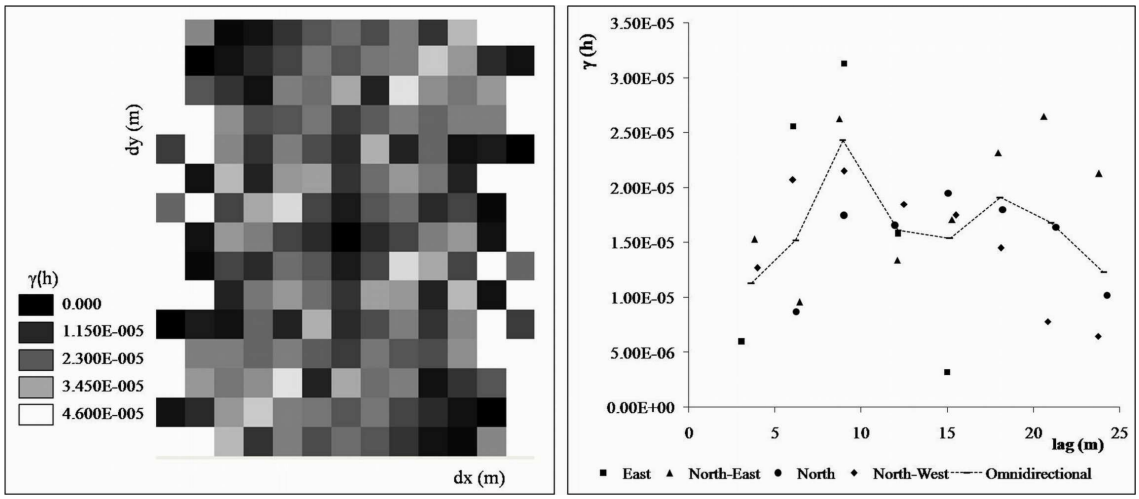

Figure 2: Variogram map (left) and directional variograms (right) of the fractal dimension variable for the RS fractal model and for high water contents. The right figure also shows the omnidirectional variogram.

Fractal model	Lag (m)	Lags num.	Variogram model	A (m)	C_1 (m_2)	C (m_2)	C_0 (m_2)
TW(I)	3	8	Spherical	11	$4.10 \cdot 10^{-5}$	$1.27 \cdot 10^{-4}$	$8.60 \cdot 10^{-5}$
RS(I)	3	8	Spherical	13	$1.14 \cdot 10^{-5}$	$1.74 \cdot 10^{-5}$	$6.00 \cdot 10^{-6}$
$PSF_{0.30}$(I)	3	8	Spherical	14.5	$2.00 \cdot 10^{-4}$	$3.96 \cdot 10^{-4}$	$1.96 \cdot 10^{-4}$
$PSF_{0.45}$(I)	3	8	Spherical	15	$6.80 \cdot 10^{-5}$	$1.22 \cdot 10^{-4}$	$5.40 \cdot 10^{-5}$
$PSF_{0.60}$(I)	3	8	Spherical	14.5	$3.36 \cdot 10^{-5}$	$5.78 \cdot 10^{-5}$	$2.42 \cdot 10^{-5}$
TW(II)	2.9	8	Spherical	14	$5.20 \cdot 10^{-4}$	$6.70 \cdot 10^{-4}$	$1.50 \cdot 10^{-4}$
RS(II)	2.8	8	Spherical	12	$8.70 \cdot 10^{-6}$	$1.72 \cdot 10^{-5}$	$8.50 \cdot 10^{-6}$
$PSF_{0.30}$(II)	2.8	8	Spherical	13	$8.30 \cdot 10^{-3}$	$1.31 \cdot 10^{-2}$	$4.80 \cdot 10^{-3}$
$PSF_{0.45}$(II)	2.8	8	Spherical	12	$1.55 \cdot 10^{-4}$	$2.69 \cdot 10^{-4}$	$1.14 \cdot 10^{-4}$
$PSF_{0.60}$(II)	2.8	8	Spherical	12	$4.90 \cdot 10^{-5}$	$7.70 \cdot 10^{-5}$	$2.80 \cdot 10^{-5}$

Table 4: Results of structural analysis for each data set of fractal dimension variable.

Fractal Model	ME	VSE	Fractal Model	ME	VSE
TW(I)	$2.53 \cdot 10^{-4}$	1.0089	TW(II)	$-1.99 \cdot 10^{-4}$	1.0048
RS(I)	$4.7 \cdot 10^{-5}$	1.0056	RS(II)	$-1.31 \cdot 10^{-4}$	1.0018
$PSF_{0.30}$(I)	$7.22 \cdot 10^{-4}$	1.0035	$PSF_{0.30}$(II)	$-2.1 \cdot 10^{-4}$	1.0166
$PSF_{0.45}$(I)	$2.80 \cdot 10^{-4}$	1.0042	$PSF_{0.45}$(II)	$-2.95 \cdot 10^{-4}$	1.0084
$PSF_{0.60}$(I)	$1.69 \cdot 10^{-4}$	1.0008	$PSF_{0.60}$(II)	$-2.0 \cdot 10^{-4}$	1.0171

Table 5: Results of cross-validation. The table gives the ME and VSE values for each data set.

others models, respectively. The lags number is 8 for all the data sets, then the experimental variogram furnishes a spatial correlation of measured points around 22.4 and 24 metres. The assumed type of model is the result of the cross-validation that will be treated later. The selected spherical models are characterized by a range value between 11 metres and 15 metres for the first range of scaling. For the second range this parameter varies between 12 metres and 14 metres. The sill varies between $1.22 \cdot 10^{-4}$ and $1.74 \cdot 10^{-5}$ for the first range of scaling, whereas for the other condition it assumes $1.31 \cdot 10^{-2}$ and $7.7 \cdot 10^{-5}$. The nugget is included between $1.96 \cdot 10^{-4}$ and $6 \cdot 10^{-6}$ for fractal models with high water contents; this parameter varies between $4.8 \cdot 10^{-3}$ and $8.5 \cdot 10^{-6}$ for low water contents.

The experimental variograms and the respective models with the equations are shown in Figure 3. Afterwards, Table 5 gives the results of cross-validation. It shows that for each data set of fractal dimension the *ME* and *VSE* values are very near to 0 and 1, respectively.

Then the selected variogram models represent good functions that interpolate the experimental variograms. The results are reported for all fractal models with high and low water contents.

To represent the spatial variability of fractal dimension an interpolation of the available data by ordinary kriging was performed to estimate the values where measures are not available. Selecting an opportune grid (0.25 x 0.25 metres) for the examined surface, the interpolation in each node of this was carried out to obtain the variable values in each of these nodes. The maps of the fractal dimension variable for each fractal model with high and low water contents are shown in Figs. 4 and 5

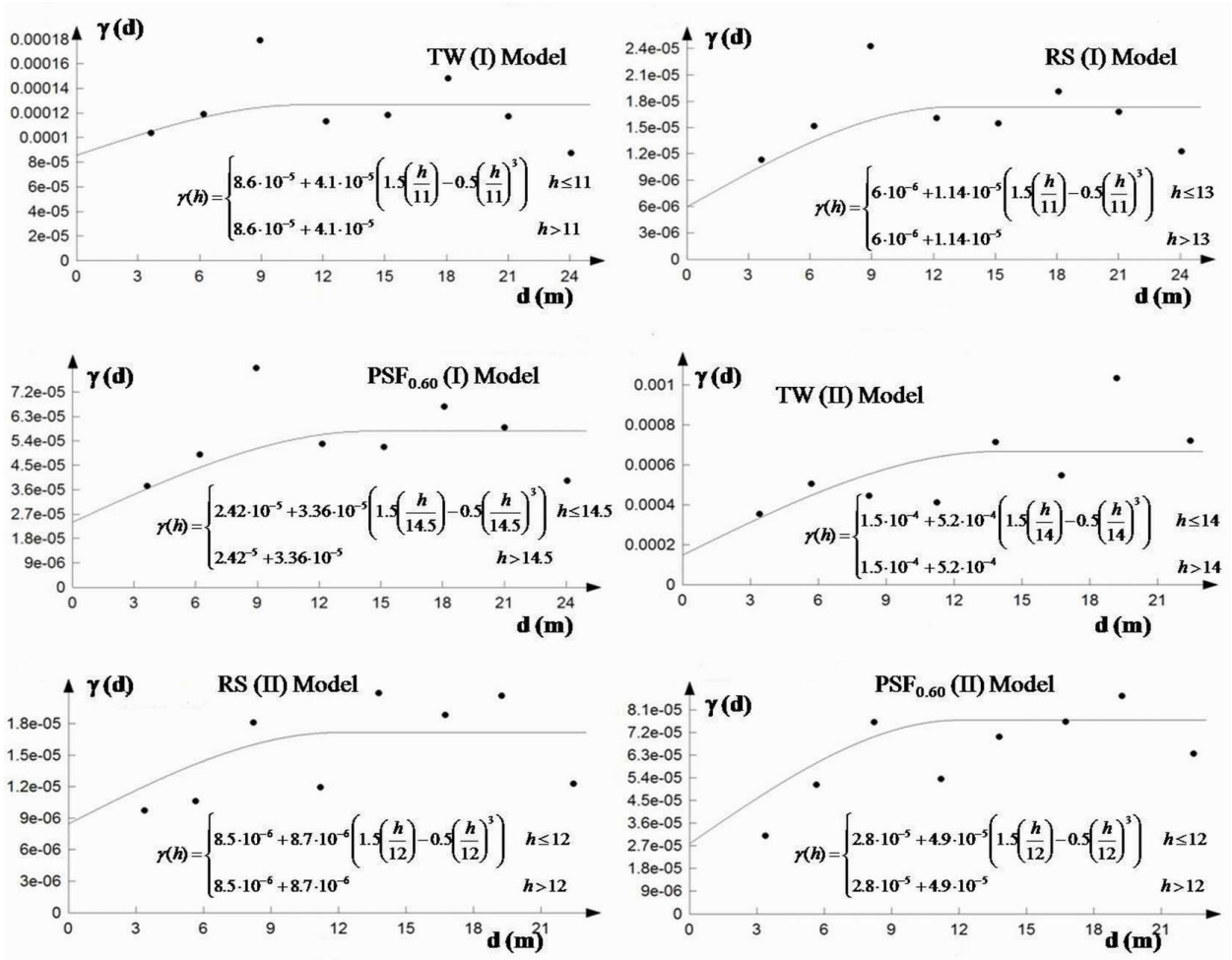

Figure 3: Experimental variograms and models for TW, RS and PSF with *A*=0.60 fractal models for high and low water contents. These plots also show the equations of spherical variogram models for each data set of fractal dimension variable.

respectively.

D_f assumes values between 2.9314 and 2.9779 for high water contents in the TW model; it has low values in two zones of the considered area and, precisely, in the South-West and North-West parts. The highest values, between 2.96 and 2.9779, characterise all the central area and a small zone to the South-East. The D_f variable varies between 2.7423 and 2.8362 for the same fractal model and for low water contents; in this case all the area has very low values (between 2.7423 and 2.78) except for the North zone and a small portion located in the South-West of this area.

Examining the RS fractal model, the D_f variable has values between 2.9760 and 2.9931 and between 2.9388 and 2.9538 for high and low water contents respectively; in the first case, it has the lowest values in the North part of the site and in a small South-West zone . The greatest values of D_f variable (2.987÷2.99), as for the TW model, were estimated in the central and South-East zones. In the second case, the examined area shows the highest values in the North and South-East portions, whereas the remaining area is characterised by very low values.

For the PSF fractal model with A=0.30 and for the first range of scaling, fractal dimension assumes values between 2.8959 and 2.9731; the smaller values are in the South-West and North-East parts of the site whereas the greatest values are in the South-East and the central zones. Considering the second range of scaling, the D_f variable has values between 2.3291 and 2.6960; observing the map, in this case D_f assumes the lowest values (between 2.3329 and 2.45) in South-West and central parts of the site; in the remaining area there are the greater values.

For the PSF with A=0.45 model the D_f variable has values between 2.9394 and 2.9834 and between 2.8063 and 2.8599 for the high and low water contents respectively. In the first case it is possible to see the presence of very low values in the North part and in a South-West small area; the highest values are in the central and in the South-East zones. The fractal dimension has very high values in the North-West and South-East zones for low water contents; the smaller values are in the South-West area and in a small zone of the experimental site.

Finally, for the PSF with A=0.60 model, D_f has values between 2.9572 and 2.9880 for the high water contents; it has low values in two zones of the study area and,

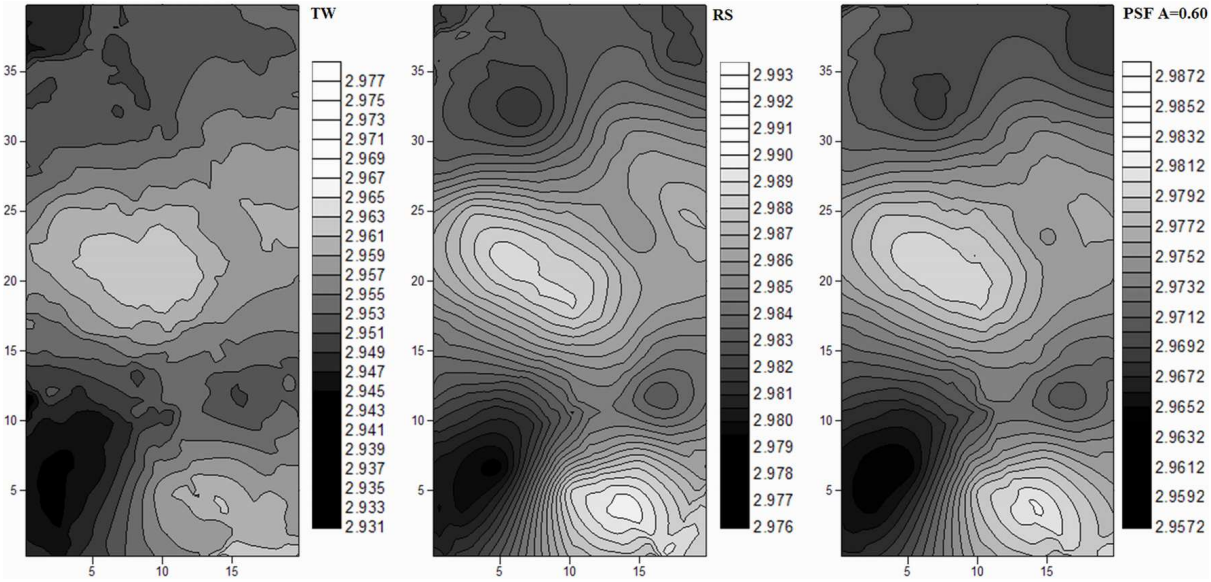

Figure 4: Maps of the D_f variable for high water contents and for the TW, RS and PSF with *A*=0.60 fractal models.

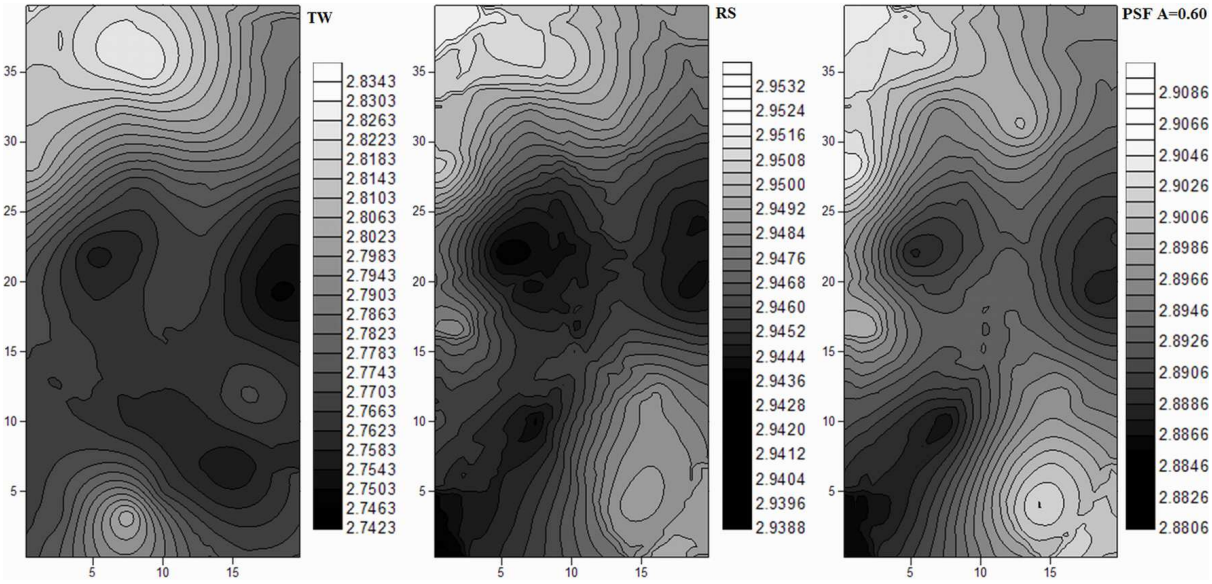

Figure 5: Maps of the D_f variable for low water contents and for the TW, RS and PSF with *A*=0.60 fractal models.

precisely, in the Northern and South-West parts. The highest values characterize the central and South-East zones. For the same fractal model and for low water contents, D_f varies between 2.8806 and 2.9101; in this case the experimental site has very low values in the central and South-West areas whereas the highest values are in the South-East and North-West parts.

After spatial interpolation by ordinary kriging, it is essential to evaluate the error and the accuracy of prediction (evaluation of ordinary kriging variance) related to each location and for all the fractal models. Fig. 6 gives these results by the normalized error and variance for the locations 1, 11, 22, 28 and for high water contents. They show that for all the locations (except n. 28) the RS model has the smallest error values whereas the highest errors characterize the TW and PSF with A=0.30 fractal models. In some locations, the fractal dimension variable was overestimated with respect to locally calculated values. Fig. 6 shows this comparison for each model and for some among the most significant locations.Specifically, at location 22 the fractal dimension was overestimated for the TW and RS models, whereas this variable was underestimated for all the PSF models. Finally, examining location 28, the PSF model with A=0.30 is the only model that has a larger estimate value with respect to the calculated values.

Fig. 7 gives the same results for locations 2, 11, 26, 29 and for low water contents. The results of the variance values show a very explicit condition: in the RS fractal model the accuracy of prediction proves the best, whereas the PSF model with A=0.30 appears the least reliable. In the same Fig. 7, the graph relative to loca-

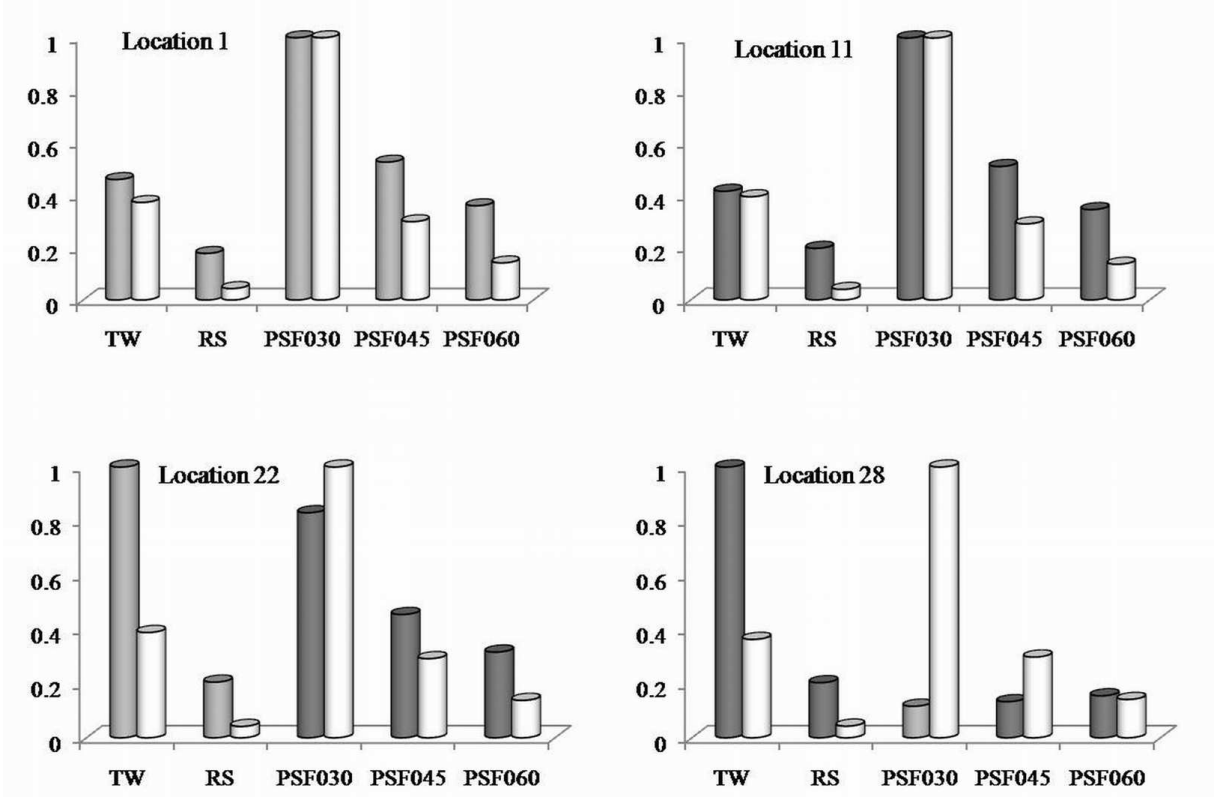

Figure 6: The errors and the kriging variance normalized values for some among the most significant locations (1, 11, 22, 28) and for each fractal model. The results are for high water contents. The clear gray histograms represent overestimation of the fractal dimension; the dark gray histograms indicate an underestimation of the variable. The variance values are represented by white histograms.

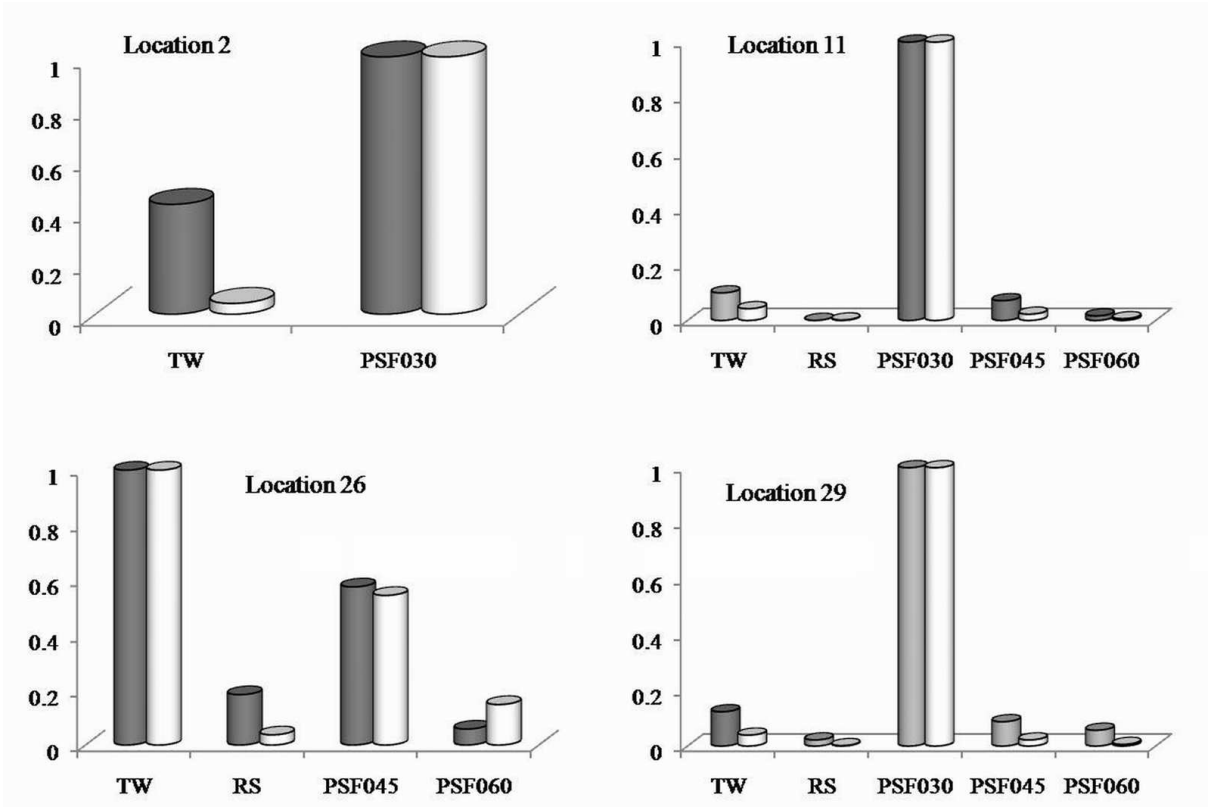

Figure 7: The errors and the kriging variance normalized values for some among the most significant locations (2, 11, 26, 29) and for each fractal model. The results are for low water contents. The clear gray histograms represents an overestimation of the fractal dimension; the dark gray histograms indicate the underestimation of the variable. The variance values are represented by white histograms.

tion 2, the results concern the TW and PSF with A=0.30 fractal models, respectively, because for the other models at the same location the fractal dimension proves to be an outlier value. For the same reason, at location 26 analogous considerations were made for the PSF with A=0.30 model. Examining these results it is possible to see that the RS model shows the lower error value for all the locations whereas the highest errors concern above all the PSF model with A=0.30, except for locations 22, 23, 26 for which the TW fractal model is the least reliable.

These results show that there are important differences between high and low water contents. Examining all the fractal models for the first case, at each location, there is often a similar condition of overestimation and/or underestimation of the fractal dimension. This condition does not exist for the low water contents, because there are locations in which the estimate value is greater than the measured value for a single fractal model whereas for the others it is contemporarily smaller.

Conclusions

The application of geostatistical methods to the fractal dimension, obtained with the scaling of some fractal models to predict WRC, permitted quantification of the value of this variable on all the area of the experimental site without the measure. The results can be used in various applications, particulary in flow predictions and transport processes on the field scale. Each WRC can be divided into two scaling ranges of scaling, lower and upper, respectively for low and high water contents [25]. There were ten data sets used, five samples are related to the low scaling range and the others to the high scaling range. These data sets can be described with a normal and log-normal distribution. Geostatistical analysis was applied to each sample to evaluate the behavior of fractal dimension in an experimental site of the Turbolo basin (a tributary of the Crati River) located in Calabria, Italy.

The spatial distribution of the fractal dimension on this area was obtained with ordinary kriging that is an exact interpolation technique, which assumes the local stationary of the mean. A strong equality of the spatial distribution of the variable was verified for high water contents, because the maps show many similarities between all the fractal models, whereas there is a great inequality for low water contents, because the maps of the models present different features. This difference depends on the number of experimental points regarding the low water content range of scaling that proves to be very limited.

The RS model shows the best fitting of the measured values for the first and second range of cut-off scaling, because it often presents the smallest error value and the kriging variance related assumes lesser values at many locations. Compared to the previous study of Fallico et al. [25], this work shows a more detailed geostatistical analysis performing the evaluation of possible anisotropies. However, the results of this study confirm the conclusions of the previous work [25], because the RS proves to be the best fractal model to interpret the true values for both high and low water contents.

References

[1] Anderson, A. N.; McBratney, A. B. 1995. “Soil aggregates as mass fractals”. *Australian Journal of Soil Research*, 33 (5): 757-772.

[2] Tyler, S. W.; Wheatcraft, S. W. 1989. “Application of fractal mathematics to soil water retention estimation”. *Soil Society of American Journal*, 53 (4): 987-996.

[3] Perfect, E.; Kay, B. D. 1991. “Fractal theory applied to soil aggregation”. *Soil Science Society of American Journal*, 55 (6): 1552-1558.

[4] Crawford, J. W.; Sleeman, B. D.; Young, I. M. 1993. “On the relation between number-size distribution and the fractal dimension of aggregates”. *Journal of Soil Science*, 44 (4): 555-565.

[5] Toledo, G.; Novy, R. A.; Davis, H. T.; Scriven, L. E. 1990. “Hydraulic conductivity of porous media at low water content”. *Soil Science Society of American Journal*, 54 (3): 673-679.

[6] Katz, A. J.; Thompson, A. H. 1985. “Fractal sandstone pores: implications for conductivity and pore formation”. *Physical Review Letters*, 54 (12): 1325-1327.

[7] Bird, N.; Bartoli, F.; Dexter, A. R. 1996. “Water retention models for fractal soil structure”. *European Journal of Soil Science*, 47 (1): 1-6.

[8] Rieu, M.; Sposito, G. 1991a. “Fractal fragmentation, soil porosity and soil water properties: I. Theory”. *Soil Science Society of American Journal*, 55 (5): 1231-1238.

[9] Rieu, M.; Sposito, G. 1991b. “Fractal fragmentation, soil porosity and soil water properties: II. Applications”. *Soil Science Society of America Journal*, 55 (5): 1239-1244.

[10] Crawford, J. W.; Ritz, K.; Young, I. M. 1995. “The relation between the moisture-release curve and the structure of soil”. *European Journal of Soil Science*, 46 (3): 369-375.

[11] Perrier, E.; Rieu, M.; Sposito, G.; Marsily, G. 1996. “Models of the water retention curve for soils with a fractal pore size distribution”. *Water Resources Research*, 32 (10): 3025-3031.

[12] Bird, N.; Perrier, E.; Rieu, M. 2000. “The water retention function for a model of soil structure with pore and solid fractal distributions”. *European Journal of Soil Science*, 51 (1): 55-63.

[13] Matheron, G. 1971. “The theory of regionalized variables and its applications”. *Les Cahiers du Centre de Morphologie Mathématique, Fascicule 5. Centre de Géostatistique, Fontainableau, France*, 212.

[14] Journel, A. G.; Huijbregts, C. J. 1978. "Mining Geostatistics". *London, ENGLAND: Academic Press*.

[15] Deutsch, C. V.; Jounel, A. G. 1998. "GSLIB Geostatistical Software Library and User's Guide". *New York, USA: Oxford University Press*.

[16] Isaaks, E. H.; Srivastava, M. 1989. "An Introduction to Applied Geostatistics". *New York, USA: Oxford University Press*.

[17] Hunt, A. G. 2004. "Continuum percolation theory for pressure-saturation characteristics of fractal soils: extension to non-equilibrium". *Advances in Water Resources*, 27 (3): 245-257.

[18] Perfect, E. 2005. "Modeling the primary drainage curve of prefractal porous media". Vadose Zone Journal, 4 (4): 959-966.

[19] Perfect, E.; Kenst, A. B.; Dìaz-Zorita, M.; Grove, J. H. 2004. "Fractal analysis of soil water desorption data collected on disturbed samples with water activity meters". *Soil Science Society of America Journal*, 68 (4): 1177-1184.

[20] Tyler, S. W.; Wheatcraft, S. W. 1990. "Fractal processes in soil water retention". *Water Resources Research*, 26 (5): 1047-1054.

[21] Danielson, R. E.; Sutherland, P. L. 1986. "Porosity. In: Methods of Soil Analysis, Part 1, Physical and Mineralogical Methods". *American Society of Agronomy*: 443-461.

[22] Perrier, E.; Bird, N.; Rieu, M. 1999. "Generalizing the fractal model of soil structure: the PSF approach". *Geoderma*, 88 (3-4): 137-164.

[23] Wang, K.; Zhang, R.; Wang, F. 2005. "Testing the pore-solid fractal model for the soil water retention function". *Soil Science Society of America Journal*, 69 (3): 776-782.

[24] Millàn, H.; Gonzàles-Posada, M. 2005. "Modelling soil water retention scaling. Comparison of a classical fractal model with a piecewise approach". *Geoderma*, 125 (1-2): 25-38.

[25] Fallico, C.; Tarquis, A. M.; De Bartolo, S.; Veltri, M. 2010. "Scaling analysis of water retention curves for unsaturated sandy loam soils by using fractal geometry". *European Journal of Soil Science*, 61 (3): 425-436.

[26] Meakin, P. 1998. "Fractals, Scaling and Growth Far From Equilibrium". *Cambridge, ENGLAND: Cambridge University Press*.

[27] Matheron, G. 1963. "Principles of geostatistics". *Economic Geology*, 58 (8): 1246-1266.

[28] Tobler, W. 1970. "A computer movie simulating urban growth in the Detroit region". *Economic Geography*, 46 (2): 234-240.

[29] Barnett, V.; Lewis, T. 1978. "Outliers in Statistical Data". *New York, USA: John Wiley and Sons*.

[30] Dixon, W. J. 1953. "Processing Data for Outliers". *Biometrics*, 9 (1): 74-89.

[31] Davis, C. J. 1973. "Statistics and Data Analysis in Geology". *New York, USA: John Wiley & Sons*.

[32] Kolmogorov, A. N. 1933. "Foundations of the Theory of Probability". *New York, USA: Chelsea Publishing Company*.

[33] Anderson, T. W.; Darling, D. A. 1952. "Asymptotic theory of certain goodness of fit criteria based on stochastic processes". *Annals of Mathematical Statistics*, 23 (2): 193-212.

[34] Kitanidis, P.; Vomvoris, E. 1983. "A geostatistical approach to the inverse problem in ground water modeling (steady state) and one dimensional simulations". *Water Resource Research*, 19 (3): 677-690.

[35] Armstrong, M. 1998. "Basic Linear Geostatistics". *Berlin, GERMANY: Springer Verlag*.